Chinese Chemical Letters 33 (2022) 1425–1429

Contents lists available at ScienceDirect

Chinese Chemical Letters

journal homepage: www.elsevier.com/locate/cclet

# Low temperature fabrication for high-performance semitransparent $CsPbI_2Br$ perovskite solar cells

Xiaogang Yang[a], Jiejia Han[a,b], Wei Ruan[c], Yanqiang Hu[b,c,d,*], Zhengyan He[b], Xiangrui Jia[b], Shufang Zhang[b,*], Dehua Wang[b,*]

[a] College of Environment and Safety Engineering, Qingdao University of Science & Technology, Qingdao 266042, China
[b] School of Physics and Photoelectronic Engineering, Ludong University, Yantai 264025, China
[c] College of Materials Science and Engineering, Nanjing University of Science & Technology, Nanjing 210094, China
[d] College of Chemistry and Chemical Engineer, Nantong University, Nantong 226001, China

ARTICLE INFO

*Article history:*
Received 30 June 2021
Revised 7 August 2021
Accepted 9 August 2021
Available online 12 August 2021

*Keywords:*
$CsPbI_2Br$ perovskite
$\gamma$-Aminobutyric acid
Stability
Low-temperature fabrication
Semitransparent solar cells

ABSTRACT

All-inorganic $CsPbI_2Br$ perovskite with suitable bandgap and excellent thermal stability has been reported as the most promising candidate for efficient perovskite solar cells (PSCs). However, the high annealing temperature (> 250 °C) and poor stability of $\alpha$-$CsPbI_2Br$ greatly limit the future application in photovoltaic field. Herein, a facile method is reported to prepare $\alpha$-$CsPbI_2Br$ perovskite film with high stability at low temperature (70 °C) by incorporating a small amount of $\gamma$-aminobutyric acid (GABA) in the precursor solutions. The devices exhibit reproducible photovoltaic performance with a champion efficiency up to 15.16%, along with the excellent stability, maintaining more than 80% of its initial efficiency after stored in ambient condition for 600 h without any encapsulation. Most importantly, the method enables fabrication of semitransparent $CsPbI_2Br$ PSCs with a PCE of 6.76%, as well as an average visible transparency (AVT) of 25.38%. To the best of our knowledge, this is the first attempt to apply $CsPbI_2Br$ to the semitransparent solar cells.



Organic-inorganic halide perovskites have attracted enormous research interest in the photovoltaic community for their excellent performance as light harvesters [1-5]. Benefited from their outstanding optical properties, the power conversion efficiency (PCE) of solar cells based on organic-inorganic halide has exceeded 25% in merely one decade [6,7]. However, the poor long-term stability is still the major obstacle hindering commercial applications of organic–inorganic halide perovskite solar cells (PSCs) due to the intrinsic volatile and hydrophilic nature of the organic components in the hybrid perovskite framework, especially for the commonly used organic cations such as methylammonium ($MA^+$) and formamidinium ($FA^+$) [8,9]. Alternatively, replacing the organic cations with inorganic caesium cation ($Cs^+$) to build all-inorganic cesium lead halide perovskites ($CsPbX_3$, X = I, Br, Cl or mixed halides) has been proved to be a feasible and effective approach for improving the thermal stability [10-12].

Among the cesium lead halide perovskites, $CsPbI_2Br$ has attracted the most attention because of its balancing the trade-off between band gap (~1.90 eV) and phase stabilization [13]. Currently, the $CsPbI_2Br$-based solar cells have achieved PCE exceeded 17% and exhibited excellent stability, indicating a great potential for industrial applications, especially as top cells for tandem solar cells [14]. However, the cubic $CsPbI_2Br$ ($\alpha$-phase) is still a metastable phase at room temperature, and can easily convert to a non-perovskite orthorhombic phase ($\delta$-phase) when exposed to high humidity [15,16]. To stabilize the cubic $\alpha$-$CsPbI_2Br$ phase, several methods such as reducing grain size [17], enhancing film quality [18] and doping other elements [19,20] have been explored. On the other hand, the $\alpha$-$CsPbX_3$ perovskites usually require high-temperature annealing (> 250 °C) for obtaining the $\alpha$-phase, which not only increases energy consumption but also greatly limits the applications in multi-junction tandem and flexible devices. Recently, several approaches have been attempted to prepare $\alpha$-$CsPbI_2Br$ at low annealing temperature, such as using $HPbI_3$ in the precursor to instead of $PbI_2$ to lower the annealing temperature at 130 °C [21], and using a Lewis base to promote the growth process of $\alpha$-$CsPbI_2Br$ films at 120 °C [22]. However, it is still challenging to obtain high-quality $\alpha$-$CsPbI_2Br$ with long-term stability *via* low-temperature solution-processed methods.

* Corresponding authors.
*E-mail addresses:* huyqntu@ntu.edu.cn (Y. Hu), ZSF2013CPO@163.com (S. Zhang), lduwdh@163.com (D. Wang).

https://doi.org/10.1016/j.cclet.2021.08.039
1001-8417/

Herein, we demonstrate that $\gamma$-aminobutyric acid (GABA), a common amino acid in the human body, can be used as an effective additive to obtain $\alpha$-$CsPbI_2Br$ perovskite with long-term stability at a low annealing temperature of 70 °C (the lowest annealing temperature for $\alpha$-$CsPbI_2Br$ ever report). It was found that the GABA molecules can effectively retard the fast crystallization of $CsPbI_2Br$ and reduce size of the coordination colloidal framework by interacting with ions and colloids in the precursors, and thus could help to obtaining a high quality $\alpha$-$CsPbI_2Br$ film as well as excellent moisture stability. The solar cells based on the obtained $\alpha$-$CsPbI_2Br$ films achieved a highest PCE of 15.16%, which is comparable to the $CsPbI_2Br$ solar cells fabricated at much higher annealing-temperature. Furthermore, this approach also show great potential in fabricating semitransparent perovskite solar cells, which are promising for some special application such as photovoltaic curtains, building-integrated photovoltaics, wearable electronics, and tandem cells [23-25]. Consequently, we obtained a well-designed semitransparent solar with a PCE of 6.76%. This work not only provides a feasible route for preparing high-quality $CsPbI_2Br$ perovskites at low temperature but also represents an important step for their application in high-performance and low-cost semitransparent electronics.

Cesium iodide (CsI, 99.9%), lead iodide ($PbI_2$, 99.9%), lead bromine ($PbBr_2$, ≥ 98%), $\gamma$-aminobutyric acid (GABA, 99.9%), titanium diisopropoxide bis(acetylacetonate) (75% inisopropanol), and dimethyl sulfoxide (DMSO, anhydrous, 99.8%) were purchased from Sigma-Aldrich. All salts and solvents were used as purchased without any further purification.

For the one-step solution method, the $CsPbI_2Br$ perovskite precursor solution was prepared by dissolving CsI (0.25982 g), $PbI_2$ (0.2035g), $PbBr_2$ (0.1835g) powder, and a certain amount (0 mol%, 1 mol%, 3 mol%, 5 mol%, 10 mol%, mole ratio of GABA to $CsPbI_2Br$) of GABA in 1 mL DMSO solvent and then stirred at 70 °C overnight in a nitrogen-filled glove box. And a Fluorine-doped tin oxide (FTO) conducting glass (2 cm × 2cm, sheet resistance about 8 ohm/square) was ultrasonically cleaned by detergent, deionized water, and acetone for 30 min sequentially, and then treated by a $UV/O_3$ cleaner for 15 min. Then, a uniform dense $TiO_2$ layer was deposited on the substrate by spin coating 0.15 mol/L titanium diisopropoxide bis (acetylacetonate) in butanol at 3500 rpm and repeating the process for twice, and then sintering at 500 °C for 2 h. Then the perovskite layer was deposited on the glass/FTO/compact $TiO_2$ by the spin-coating the as-prepared precursor solution at 1000 rpm for 10 s and 3500 rpm for 35 s. Sequentially, the spin coated film was annealing at 70 °C for 5 min to form the perovskite film. Then, the film was covered by the hole transporter spiro-OMeTAD (99.5%, Xi'an Polymer Light Technology Corp). 0.167 g spiro-OMeTAD was dissolved in 1.00 ml chlorobenzene, and 0.0103 g LiTFSI and 0.0298 g *tert*-butylpyridine (TBP) were used as additives and then the solution was deposited by spin-coating at 6500 rpm for 30 s. Finally, a 100-nm thick Au electrode was deposited on top of the device by thermal evaporation under *ca.* $1 \times 10^{-6}$ torr vacuum condition, through a shadow mask. For the semitransparent PSCs, the first few steps are the same, but the last step replaces Au electrode with Ag nanowires by spin-coating.

Powder X-ray diffraction (XRD) patterns of the perovskite films were recorded by a Bruker D8 diffractometer with Cu K$\alpha$ radiation ($\lambda$ = 1.5406 Å). FTIR spectra were measured using a Bruker Vertex 80v Fourier transform infrared spectrometer. The surface morphology of the perovskite films was observed by field-emission scanning electron microscopy (FE-SEM; Quanta 250FEG) and atomic force microscope (AFM; Brook Multimode 8), respectively. The size distributions of the colloid cluster in perovskite precursor solutions were tested by zeta potential analyzer (Brookhaven Zeta Plus). Absorption and transmittance spectra of the prepared films were measured with an UV-vis-NIR spectrophotometer (UV-3600, Shimadzu). The visible transparency was evaluated by an ISO standard method (ISO 9050:2003) of glass in buildings. The PL spectra of the films were obtained at room temperature by using a steady-state lifetime spectrofluorometer (Varian Cary Eclipse). The time-resolved photoluminescence decay of the perovskite film was measured using a Horiba Fluorolog-3 Time Correlated Single Photon Counting (TCSPC) system with an excitation wavelength at 412 and 704 nm for orthorhombic and cubic, respectively. The current-voltage characteristic curves of the fabricated PSCs were measured under standard AM 1.5 sunlight (100 mW/cm$^2$, WXS-90L2, Wacom) with 30 mV/s scanning rate. The effective area of the cell was defined as 0.09 cm$^2$ using a non-reflective metal mask.

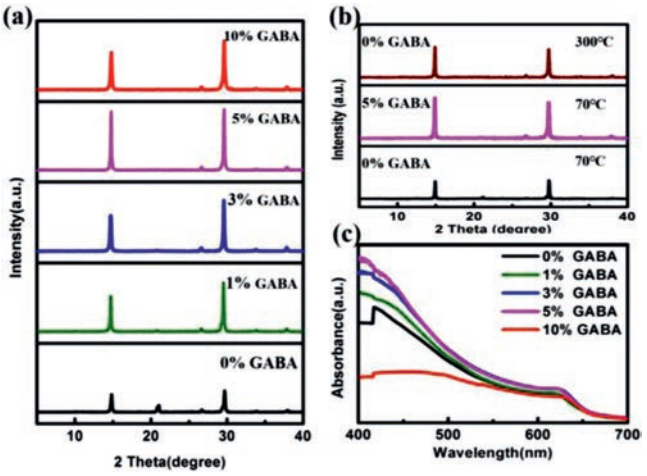


**Fig. 1.** (a) XRD patterns of $CsPbI_2Br$ perovskite films without or with different mole percentages of GABA. (b) XRD patterns of $CsPbI_2Br$ perovskite films annealing at different temperature. (c) Absorbance spectra of $CsPbI_2Br$ perovskite films without or with different mole percentages of GABA.

The $CsPbI_2Br$ films in this work were all prepared *via* a one-step spin-coating process by employing perovskite precursor solutions with adding different concentrations of GABA and followed by annealing at 70 °C for 10 min in a glovebox filled with $N_2$, the details are shown in the Experiment Section (Supporting information). Fig. S1 (Supporting information) show the chemical structure of GABA. The X-ray diffraction (XRD) patterns of the $CsPbI_2Br$ films with adding different concentrations of GABA in the precursor solutions were shown in Fig. 1a. All samples present clear diffraction peaks at 14.6° and 29.5° and are well consistent with the typical (100) and (200) planes of the $\alpha$-$CsPbI_2Br$ crystal. The absolute intensities of the (100) and (200) planes are getting stronger as the concentration of GABA increases and reach the maximum values when the concentration of GABA increases to 5 mol%, which indicates that moderate incorporation of GABA is beneficial to improve the perovskite crystallinity. As shown in Fig. 1b, with the incorporation of GABA, the $CsPbI_2Br$ film even show a little stronger crystallinity intensity than that of the one processed at high-temperature (300 °C). However, when increase the GABA concentration up to 10 mol%, the GABA molecule seems harmful to the crystallinity, showing the reduction of the peak intensity. To evaluate the optical properties of these $CsPbI_2Br$ films, the corresponding absorption spectra were shown in Fig. 1c. With the increase of GABA concentration to 5 mol%, the absorption of $CsPbI_2Br$ films gradually increased and reached the strongest absorption, which was in good agreement with the XRD patterns.

Top view SEM images of the as-prepared $CsPbI_2Br$ films (Fig. S2 in Supporting information) indicated that the incorporation of GABA greatly influences the morphology of the films. The $CsPbI_2Br$ film without GABA exhibits numerous big voids on the film sur-

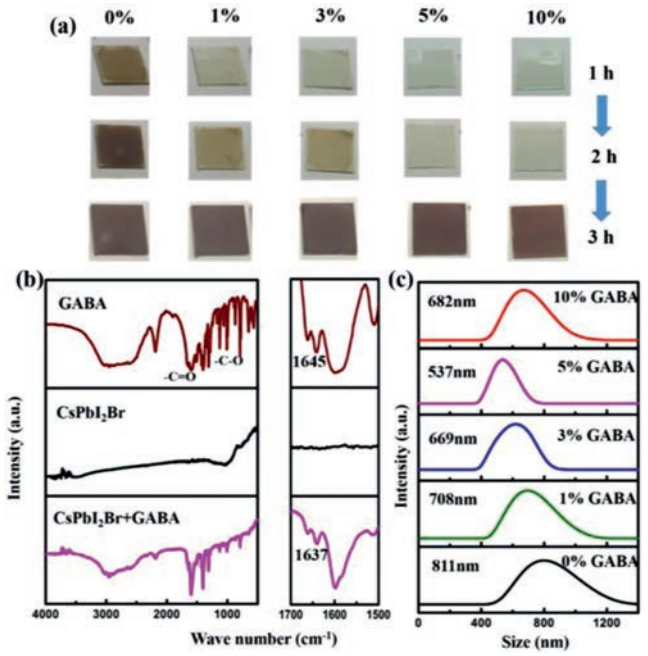


**Fig. 2.** (a) Optical images of the fresh-coated $CsPbI_2Br$ perovskite films without or with different mole percentages of GABA stored in glovebox as a function of time. (b) FTIR spectroscopy characterization of GABA, $CsPbI_2Br$ and a complex of both. (c) Size distributions of the colloidal particles in $CsPbI_2Br$ solutions mixed with different mole percentages of GABA.

face, which could greatly influence the photoelectric performance. After incorporating 1 mol% GABA into the precursor solution, voids on the surface became less and smaller. Better coverage of the film surface was obtained when the GABA concentration was gradually increased to the optimum value of 5 mol%, which is highly consistent with the results of XRD spectra. However, with further increase of GABA, the film surface became uneven and non-uniform.

To investigate the mechanism of GABA molecule affecting the crystallization process of $CsPbI_2Br$ films, we observed the color changing process of the films without annealing. As shown in Fig. 2a, the film without GABA changed to light brown in a short time, suggesting the formation of perovskite crystals. In contrast, the fresh films incorporating with different concentration of GABA are almost transparent in 1 h. The color of the films with low concentration of GABA gradually changed into light brown after 1 hour, while the films with 5 mol% and 10 mol% GABA still kept transparent after 2 h. This observation clearly indicated the incorporation of GABA can effectively retard the rapid crystallinity of $CsPbI_2Br$, which facilitates to form uniform perovskite films with excellent crystallinity [26,27]. In order to verify the interaction of GABA with cations in the precursor solution, we carried out Fourier transform infrared spectroscopy (FTIR) measurements and tested the size distributions of colloidal particles *via* a zeta potential analyzer. As shown in Fig. 2b, a strong peak was observed at 1645 $cm^{-1}$ in the FTIR spectrum of GABA powder, which can be ascribed to the typical stretching of group C=O. The C=O vibration band of the $CsPbI_2Br$ films incorporated with GABA molecule was shifted to 1637 $cm^{-1}$, indicating an interaction between functional groups of GABA and cations in the precursor [28-30]. In addition, $^1H$ NMR spectra were also used to examine the interaction of GABA with cations in DMSO-$d_6$ (Fig. S3 in Supporting information), which shows a slight chemical shift compared with pure GABA, implying a stronger interaction between GABA and perovskite precursors. Further proof for the interaction between GABA molecules and the cations was that the average size of colloids in the precursor solution was gradually reduced while increasing the GABA concentration in the precursor solution, which was revealed by testing the size distributions of colloidal particles *via* a zeta potential analyzer (Fig. 2c). On the other hand, the XRD patterns of the no-annealing films with or without GABA after spin-coating were shown in Fig. S4 (Supporting information), the obvious XRD diffraction peaks were observed in the spun films without GABA, indicating the quick crystallization of $\delta$-phase at room temperature without annealing. In contrast, the spun film with GABA was in an amorphous phase without any obvious XRD peaks except the peaks of the substrate. This demonstrated that the GABA molecules can effectively suppress the rapid crystallization of $CsPbI_2Br$.

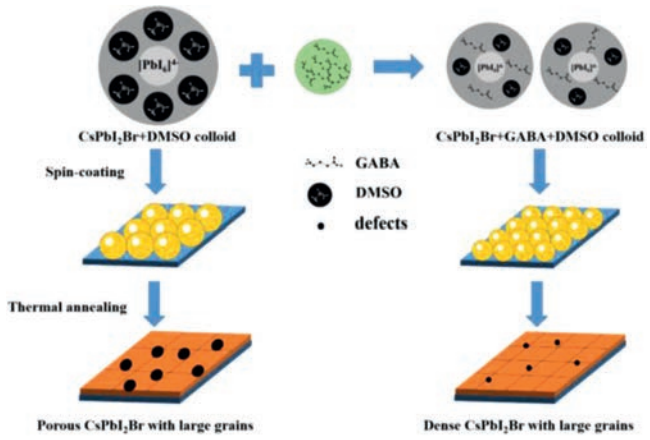


**Fig. 3.** Mechanism of GABA-induced high quality of $CsPbI_2Br$ films.

According to the test results, we propose a probable grain formation process of the $CsPbI_2Br$ films, as illustrated in Fig. 3. In the $CsPbI_2Br$ precursor solution without GABA incorporation, $Pb[I/Br]_2$ coordinated with DMSO molecules forming a crystallized $Pb[I/Br]_2{\cdot}(DMSO)_x$ colloid [26,31]. With the addition of GABA, the structure of the $Pb[I/Br]_2{\cdot}(DMSO)_x$ colloids may change to a new $Pb[I/Br]_2{\cdot}(DMSO)_x{\cdot}(GABA)_y$ structure due to the interaction between GABA and $Pb[I/Br]_2$. In the meanwhile, free GABA molecules among $Pb[I/Br]_2{\cdot}(DMSO)_x$ colloids further suppressed the combination of $Pb[I/Br]_2{\cdot}(DMSO)_x$ colloids with $Cs^+$, and the crystallization speed of $CsPbI_2Br$ was lowed. Consequently, with the help of GABA, smoother $CsPbI_2Br$ films were formed with smaller grains and less defects [32-34], which is consistent with the results of SEM and AFM (Figs. S2 and S5 in Supporting information).

We further carried out time-resolved photoluminescence (TRPL) decay measurements to investigate carrier lifetime of the $CsPbI_2Br$ films with and without GABA with a configuration of glass/perovskite. As shown in Fig. 4a, the decay curves well fitted with single-exponential components. A longer average PL decay time of the $CsPbI_2Br$ film with GABA (12.4 ns) than that of the pure $CsPbI_2Br$ film (9.7 ns) was observed. The prolonged PL decay time of the $CsPbI_2Br$ film was the result of suppressed non-radiative recombination channels in the perovskite film. To evaluate the photovoltaic performance of the devices based on the $CsPbI_2Br$ films, we further fabricated regular planar PSCs with the configuration of $FTO/TiO_2/CsPbI_2Br/Spiro\text{-}OMeTAD/Au$. The current density-voltage (*J-V*) curves of the devices based on the $CsPbI_2Br$ film without and with 5 mol% GABA are shown in Fig. 4b and the corresponding photovoltaic parameters are summarized in Table S1 (Supporting information). The pristine device with pure $CsPbI_2Br$ exhibited a relatively poor performance with a $J_{SC}$ of 14.34 $mA/cm^2$, a $V_{OC}$ of 1.17 V, a FF of 75.34%, and a PCE of 12.64%, which was due to an incomplete coverage film with low crystallinity fabricated at a low annealing temperature (70 °C). The performance of the PSCs improved gradually with the increase of incorporation of GABA (Table S2 in Supporting information). Especially, a champion PCE of

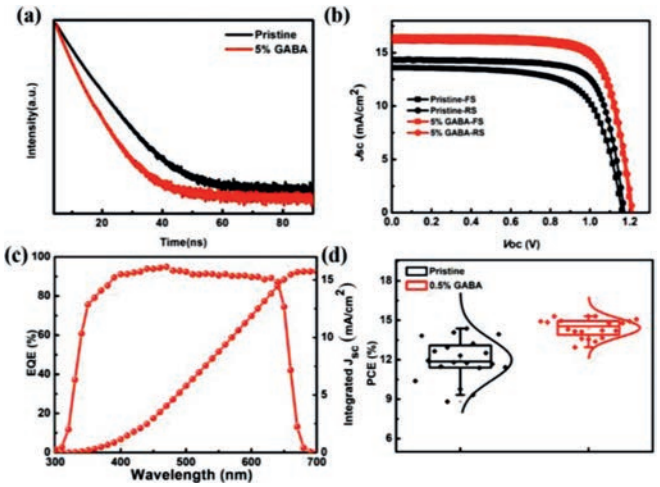


**Fig. 4.** (a) Time-resolved photoluminescence (TRPL) spectra of the films on glass. (b) *J-V* curves of pure $CsPbI_2Br$ and $CsPbI_2Br$ with 5 mol% GABA PSCs under forward (FS) and reverse scan (RS). (c) The EQE spectra and corresponding integrated $J_{sc}$ of $CsPbI_2Br$ PSCs. (d) Histogram of average efficiencies for 20 devices based on pure $CsPbI_2Br$ and $CsPbI_2Br$ with 5 mol% GABA.

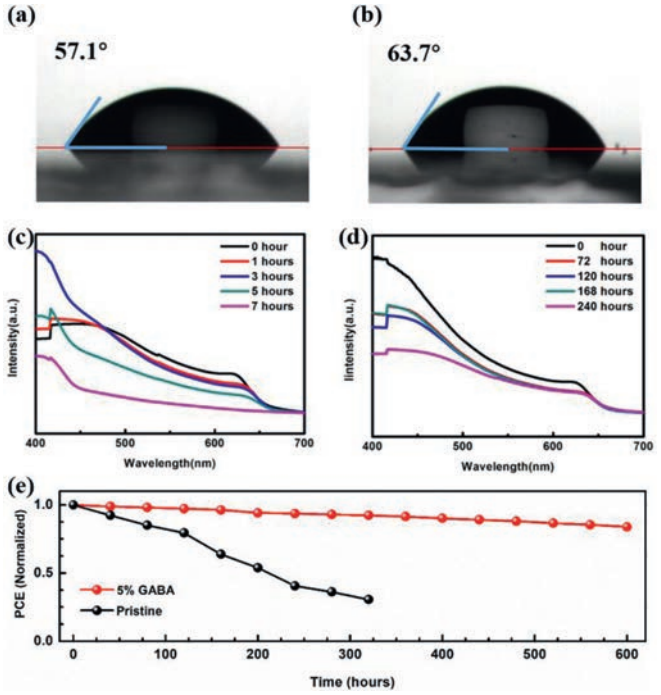


**Fig. 5.** (a) The average contact angle of the pure $CsPbI_2Br$. (b) The average contact angle of the $CsPbI_2Br$ with 5 mol% GABA. (c) The changes in absorbance with time of the pure $CsPbI_2Br$. (d) The changes in absorbance with time of the $CsPbI_2Br$ with 5 mol% GABA. (e) The normalized PCE of a device without and with 5 mol% GABA kept in an ambient environment as a function of storage time.

15.16% along with the $J_{SC}$ of 16.45 mA/cm$^2$, $V_{OC}$ of 1.21 V and FF of 76.16% were obtained with $CsPbI_2Br$ film incorporated with 5 mol% GABA. The great enhancement of the photovoltaic performance arises from the improved crystallinity and reduced non-radiative recombination in the perovskite. The hysteresis is unavoidable in inorganic PSCs with mixed halide compositions due to the iodide and bromide phase segregation under illumination [35]. In this work, a negligible *J–V* hysteresis from forward and reverse scanning of the PSCs can be observed. The external quantum efficiency (EQE) is obtained to confirm the validity of the *J–V* scan results. As shown in Fig. 4c, the integrated photocurrent density of the device with 5 mol% GABA is 15.96 mA/cm$^2$. The statistics of PCE distribution for over 30 devices demonstrated the high reliability and repeatability of the prepared PSCs (Fig. 4d).

To study the effect of GABA molecule on long-term stability, we tested the water contact angle of the controlled film and the film incorporated with 5 mol% GABA. As shown in Figs. 5a and b, after incorporating GABA, the contact angle increases from 57.1° to 63.7°, indicating that hydrophobicity of the film was improved. This was further illustrated by the atomic force microscope (AFM) images (Fig. S5). With the GABA incorporation, the prepared films obtain smoother surface of root−mean−squared (RMS) roughness from 68.4 nm to 35.6 nm, which do great favor to increasing the contact angle [36,37]. Therefore, the improved resistance against moisture of the film incorporated with 5 mol% GABA was expected. The absorption spectra of the above two kinds of films within 240 h (60% humidity, 25 °C) are shown in Figs. 5c and d, respectively. There were only slight changes in the absorption spectra of the GABA-incorporated films, while the absorption intensity of the controlled pure $CsPbI_2Br$ films significantly decreased and an obvious characteristic absorption peak of $\delta$-$CsPbI_2Br$ appeared, suggesting the $CsPbI_2Br$ partially changed from $\alpha$-phase to $\delta$-phase. Furthermore, the PCE of the GABA-incorporated cells retained more than 80% of its initial value in 600 h, while the controlled $CsPbI_2Br$ cells kept only less than 50% of its initial PCE after 200 h, as shown in Fig. 5e. We also compared the thermal stability of the prepared films incorporated with different ratio of GABA, as shown in Fig. S6 (Supporting information). After annealing at 100 °C for 1 h in ambient condition, the XRD pattern of the pure $CsPbI_2Br$ films exhibit characteristic diffraction peak of $\delta$-phase, while the compared ones with 5 mol% GABA still stay in cubic $\alpha$-phase.

During this work, we found that the 5 mol% GABA-incorporated $CsPbI_2Br$ film fabricated at low annealing temperature shows contain degree of transparency. We attempted to fabricate it into semitransparent PSCs with a configuration of FTO/$TiO_2$/$CsPbI_2Br$/Spiro-OMeTAD/Ag nanowires (Fig. S7a in Supporting information). On the basis of a ~250 nm thick GABA-incorporated $CsPbI_2Br$ film, an optimal device exhibits an average visible transparency (AVT) of 25.38% ranging from 380 nm to 780 nm (Fig. S7b in Supporting information), which is slightly higher than the required AVT for application of power-generating window of ~25% [38]. The high average transmittance of 82.6% in the infrared band exhibits a great potential application in tandem solar cells. The *J–V* characteristic shown in Fig. S7c (Supporting information) exhibits a high PCE of 6.76% for the semitransparent PSC. To the best of our knowledge, this is the first attempt to apply $CsPbI_2Br$ to semitransparent PSCs, and the performance is comparable to organic ones based on $CH_3NH_3PbI_3$ [39,40].

In summary, we developed a route to prepare $CsPbI_2Br$ with excellent performance and better stability at low temperature *via* GABA-incorporation. It was demonstrated that the GABA molecules would reduce the size of $CsPbI_2Br$ colloids by interacting with cations in the precursors and effectively suppress the rapid crystallization of $CsPbI_2Br$. Perovskite films with high quality were obtained through this way. Conventional structural PSCs based on such $CsPbI_2Br$ achieved a high PCE of 15.16% and semitransparent PSCs gain a PCE of 6.76%. This work provides a new viewpoint for understanding the phase stability of inorganic perovskites and introduces a new member to the family of semitransparent PSCs.

## Declaration of competing interest

The authors declare no competing financial interest.

## Acknowledgments

We acknowledge the financial support from the Taishan Scholar Project of Shandong Province (No. tsqn201812098), the Shandong Provincial Natural Science Foundation (Nos. ZR2020MF103, ZR2019MF057 and ZR2019MA066), National Natural Science Foundation of China (No. 21701080). The SEM and AFM experiments were performed at the Materials Characterization Facility of Nanjing University of Science and Technology.

## Supplementary materials

Supplementary material associated with this article can be found, in the online version, at doi:10.1016/j.cclet.2021.08.039.

## References

[1] L.J. Zhu, Q.P. Lu, C.H. Li, Y. Wang, Z.B. Deng, Chin. Chem. Lett. 32 (2021) 2259–2262.
[2] T. Zhu, Y.R. Yang, S.Y. Zhou, et al., Chin. Chem. Lett. 31 (2020) 2249–2253.
[3] W.L. Xu, N.S. Niu, X.Y. Yang, et al., Chin. Chem. Lett. 32 (2021) 489–492.
[4] W.D. Zhu, W.M. Chai, D.D. Chen, et al., ACS. Energy. Lett. 6 (2021) 1500–1510.
[5] M.H. Li, J.Y. Shao, Y. Jiang, et al., Angew. Chem. 133 (2021) 16524–16529.
[6] T. Ozturk, E. Akman, A.E. Shalan, S. Akin, Nano. Energy 87 (2021) 106157.
[7] NREL Chart. https://www.nrel.gov/pv/assets/pdfs/best-research-cell-efficiencies.20200922.pdf.
[8] Z.X. Wei, Y.H. Zhao, J. Jiang, et al., Chin. Chem. Lett. 31 (2020) 3055–3064.
[9] Y.H. Liu, S. Akin, L.F. Pan, et al., Sci. Adv. 5 (2019) eaaw2543.
[10] W.C. Xiang, W. Tress, Adv. Mater. 31 (2019) 1902851.
[11] M.B. Faheem, B. Khan, C. Feng, et al., ACS. Energy Lett. 5 (2020) 290–320.
[12] J.R. Zhang, G. Hodes, Z.W. Jin, S.Z. Liu, Angew. Chem. Int. Ed. 58 (2019) 15596–15618.
[13] W.C. Xiang, Z.W. Wang, D.J. Kubicki, et al., Joule 3 (2019) 205–214.
[14] S.S. Mail, J.V. Patil, P.S. Shinde, G.D. Miguel, C.K. Hong, Matter 4 (2021) 635–653.
[15] J.K Nam, M.S. Jung, S.U. Chai, et al., J. Phys. Chem. Lett. 8 (2017) 2936–2940.
[16] D.L. Bai, H. Bian, Z.W. Jin, et al., Nano Energy 52 (2018) 408–415.
[17] Z.B. Zeng, J. Zhang, X.L. Gan, et al., Adv. Energy. Mater. 8 (2018) 1801050.
[18] C.F.J. Lau, M. Zhang, X.F. Deng, et al., ACS. Energy. Lett. 2 (2017) 2319–2325.
[19] S.M. Yang, H. Zhao, Y. Han, et al., Small 15 (2019) 1904387.
[20] J.S. Zhang, C. Wang, H. Fu, et al., J. Alloys. Compd. 862 (2021) 158454.
[21] Y. Wang, T.Y. Zhang, F. Xu, Y.H. Li, Y.X. Zhao, Sol. RRL 2 (2018) 1700180.
[22] H. Jiang, J.S. Feng, H. Zhao, et al., Adv. Sci. 5 (2018) 1801117.
[23] G.E. Eperon, V.M. Burlakov, A. Goriely, H.J. Snaith, Adv. Sci. Lett. 8 (2014) 591–598.
[24] F. Guo, H. Azimi, Y. Hou, et al., Nanoscale 7 (2015) 1642–1649.
[25] J. Lin, M.L. Lai, L.T. Dou, et al., Nat. Mater. 17 (2018) 261–267.
[26] Q. Wang, X.P. Zheng, Y.H. Deng, et al., Joule 1 (2017) 371–382.
[27] G.N. Yin, H. Zhao, H. Jiang, et al., Adv. Funct. Mater. 28 (2018) 1803269.
[28] T. Qiu, Y.Q. Hu, F. Bai, X.L. Miao, S.F. Zhang, J. Mater. Chem. A 6 (2018) 12370–12379.
[29] C.M. Zhang, S.F. Zhang, X.L. Miao, et al., Part. Part. Syst. Char. 34 (2017) 1600298.
[30] B. Li, Y.N. Zhang, L. Fu, et al., Nat. Commun. 9 (2018) 1076.
[31] H.X. Rao, S.Y. Ye, F.D. Gu, et al., Adv. Energy Mater. 8 (2018) 1800758.
[32] K.Y. Yan, M.Z. Long, T.K. Zhang, et al., J. Am. Chem. Soc. 137 (2015) 4460–4468.
[33] W.Z. Li, J.D. Fan, J.W. Li, Y.H. Mai, L.D. Wang, J. Am. Chem. Soc. 137 (2015) 10399–10405.
[34] A. Swarnkar, W.J. Mir, A. Nag, ACS. Energy Lett. 3 (2018) 286–289.
[35] C. Liu, W.Z. Li, C.L. Zhang, et al., J. Am. Chem. Soc. 140 (2018) 3825–3828.
[36] T. Zhang, H. Li, S.S. Liu, et al., J. Phys. Chem. Lett. 10 (2019) 200–205.
[37] X.J. Feng, L. Jiang, Adv. Mater. 18 (2006) 3063–3078.
[38] S.P. Cho, S.I. Na, S.S. Kim, Sol. Energy Mater. Sol. Cells 196 (2019) 1–8.
[39] P. You, Z.K. Liu, Q.D. Tai, S.H. Liu, F. Yan, Adv. Mater. 27 (2015) 3632–3638.
[40] J.W. Jung, C.C. Chueh, A.K.Y. Jen, Adv. Energy Mater. 5 (2015) 1500486.